HHS Public Access

Author manuscript

NMR Biomed. Author manuscript; available in PMC 2015 July 30.

Published in final edited form as:

NMR Biomed. 2014 March ; 27(3): 240–252. doi:10.1002/nbm.3054.

Inverse *Z*-spectrum analysis for spillover-, MT-, and T_1-corrected steady-state pulsed CEST-MRI – application to pH-weighted MRI of acute stroke

Moritz Zaiss[a,*], **Junzhong Xu**[b,c], **Steffen Goerke**[a], **Imad S. Khan**[d], **Robert J. Singer**[d], **John C. Gore**[b,c,e], **Daniel F. Gochberg**[b,c,f], and **Peter Bachert**[a]

[a]Department of Medical Physics in Radiology, Deutsches Krebsforschungszentrum (DKFZ, German Cancer Research Center), Heidelberg, Germany

[b]Institute of Imaging Science, Vanderbilt University, Nashville, TN, USA

[c]Department of Radiology and Radiological Sciences, Vanderbilt University, Nashville, TN, USA

[d]Section of Neurosurgery, Geisel School of Medicine at Dartmouth, Lebanon, NH

[e]Department of Biomedical Engineering, Vanderbilt University, Nashville, TN, USA

[f]Department of Physics and Astronomy, Vanderbilt University, Nashville, TN, USA

Abstract

Endogenous chemical exchange saturation transfer (CEST) effects are always diluted by competing effects, such as direct water proton saturation (spillover) and semi-solid macromolecular magnetization transfer (MT). This leads to unwanted T_2 and MT signal contributions that lessen the CEST signal specificity to the underlying biochemical exchange processes. A spillover correction is of special interest for clinical static field strengths and protons resonating near the water peak. This is the case for all endogenous CEST agents, such as amide proton transfer, –OH-CEST of glycosaminoglycans, glucose or myo-inositol, and amine exchange of creatine or glutamate. All CEST effects also appear to be scaled by the T_1 relaxation time of water, as they are mediated by the water pool. This forms the motivation for simple metrics that correct the CEST signal.

Based on eigenspace theory, we propose a novel magnetization transfer ratio (MTR_{Rex}), employing the inverse *Z*-spectrum, which eliminates spillover and semi-solid MT effects. This metric can be simply related to R_{ex}, the exchange-dependent relaxation rate in the rotating frame, and k_a, the inherent exchange rate. Furthermore, it can be scaled by the duty cycle, allowing for simple translation to clinical protocols. For verification, the amine proton exchange of creatine in solutions with different agar concentrations was studied experimentally at a clinical field strength of 3 T, where spillover effects are large. We demonstrate that spillover can be properly corrected and that quantitative evaluation of pH and creatine concentration is possible. This proves that MTR_{Rex} is a quantitative and biophysically specific CEST-MRI metric. Applied to acute stroke

[*]Correspondence to: M. Zaiss, German Cancer Research Center (DKFZ), Department of Medical Physics in Radiology, Im Neuenheimer Feld 280, D-69120 Heidelberg, Germany. m.zaiss@dkfz.de.

induced in rat brain, the corrected CEST signal shows significantly higher contrast between the stroke area and normal tissue, as well as less B_1 dependence, than conventional approaches.

Keywords

CEST; MT; spillover; spin-lock; creatine; stroke; pH-weighted imaging

INTRODUCTION

Chemical exchange saturation transfer (CEST) exploits the chemical exchange of labile protons, either in metabolites or contrast agents, to transfer labeled magnetization to the water pool (1–3). The CEST signal is obtained by water signal acquisition after selective radiofrequency (RF) irradiation at the resonance frequency of an exchanging proton pool. Together with a reference scan, the water signal decrease caused by saturation transfer can be determined. This leads to increased sensitivity mediated by the accumulation of the labeled state in the water pool. As the labeling of the exchanging protons can be performed selectively by RF irradiation at the specific chemical shift, CEST yields biochemical information on living tissue. Several CEST-MRI approaches have been reported that enable the monitoring of cellular metabolites *in vivo*: amide proton-CEST (4), creatine-CEST (5,6), glutamate-CEST (7), glycosaminoglycan-CEST (8–10), glucose-CEST (11) and also many paramagnetic exogenous agents (3). Some exchange processes are distinctly pH sensitive and allow pH-weighted MRI (4,12–14). This makes CEST imaging interesting for the characterization of ischemic lesions as they occur in stroke where a decrease in the amide proton transfer (APT) peak has been reported (15–17).

However, the RF irradiation used for labeling also excites nearby resonances. Especially for clinical static field strengths and endogenous amide, amine and hydroxyl protons, CEST pools resonate close to the water peak with the consequence that direct saturation of the water protons surpasses the CEST effect. The impact of direct water saturation on the CEST pool resonance is called ‘spillover’. Moreover, magnetization transfer (MT) effects, owing to broad macromolecular resonances, are apparent even far away from the water peak, and overlay the CEST effect. Both spillover and MT effects increase with increasing RF irradiation amplitude B_1 (18,19). Likewise, solute labeling (and hence the possible maximum CEST effect) also increases with B_1 (20). Thus, CEST sequences are often optimized by variation of B_1 to yield maximum contrast (7,10,11), but the signal at optimal B_1 is highly sensitive to spillover (21) and correction is especially required in this optimal case. Finally, as mediated by the water pool, the water T_1 scales with the strength of the whole effect.

To assess the physiological relevance of any MRI contrast, artifacts and sources of non-specific contrast must be identified, explained and eliminated as far as possible. This problem is an active area of research in the CEST community and several approaches have been suggested to correct for the described effect: simple asymmetry analysis (4), Lorentzian line fits (22), Lorentzian differences (23,24) and more sophisticated isolation approaches, such as double-frequency irradiation (25,26) and chemical exchange rotation

transfer (CERT) (27,28). However, even CEST signals isolated from concomitant effects, such as T_2 or MT, can still be diluted by them (19,20). Thus, isolation often yields an already diluted effect, and generally does not imply spillover and MT correction: these are different issues.

Therefore, we propose a new evaluation method which is simply applicable to *Z*-spectrum data and able to both isolate and correct the effects on the CEST signal from spillover, MT and T_1. The approach uses the inverse metric of the *Z*-spectrum (1/*Z*) to obtain spillover- and MT-corrected CEST-MRI data. Our approach is based on the equivalence of spin-lock (SL) and CEST experiments (29). By employing a solution of Santyr *et al*. (30) proposed for pulsed SL, we extend this equivalence to pulsed CEST which is required in applications to clinical MR scanners. As a proof of principle, we present data from creatine–agar model solutions, but expect that this approach will be generally applicable to all types of CEST experiments driven to steady state. We also demonstrate that the inverse metric 1/*Z* is useful not only for corrections, but also for quantitative CEST-MRI. Finally, we apply the correction to APT imaging in acute stroke, where a pure exchange-weighted contrast might help in the characterization of lesions.

THEORY

The *Z*-spectrum and useful magnetization transfer ratios (MTRs) for continuous wave (cw)-CEST

We first compile results of cw theory (31,32) for two exchanging pools, the abundant pool ‘a’ (water pool) with thermal magnetization M_{0a} and the rare pool ‘b’ (CEST pool) with thermal magnetization M_{0b}. For most metabolite–water systems, an asymmetric population given by the proton fraction $f_b = M_{0b}/M_{0a} < 1\%$ can be assumed. Both pools undergo longitudinal and transverse relaxation with rates R_{1a}, R_{2a}, R_{2b}. The longitudinal relaxation of pool b, R_{1b}, is assumed to be small compared with the exchange rate, and is neglected in the following (32). The pools are coupled by the exchange rate k_b and the back exchange rate $k_a = f_b k_b$. The RF irradiation amplitude ($\omega_1 = \gamma B_1$) and offset frequency from water ($\Delta\omega$) define the off-resonant saturation, which leads to an effective field vector $\vec{\omega_{\text{eff}}} = (\omega_{\text{eff}}, 0, \Delta\omega)$ tilted by the angle $\theta = \tan^{-1}(\omega_1/\Delta\omega)$ off the *z* axis (18,22). The steady-state magnetization after saturation M_{sat}, normalized by the thermal magnetization M_{0a}, was named the *Z*-value by Woessner *et al*. (33). The *Z*-spectrum or $Z(\Delta\omega)$ is given by (32):

$$Z(\Delta\omega) = \frac{M_{\text{sat}}(\Delta\omega)}{M_{0a}} = \cos^2\theta \frac{R_{1a}}{R_{1\rho}} \quad [1]$$

where $R_{1\rho}$ is the longitudinal relaxation rate of the water pool in the rotating frame:

$$R_{1\rho} = R_{\text{eff}} + R_{\text{ex}} \quad [2]$$

R_{ex} is the exchange-dependent relaxation in the rotating frame; R_{eff} corresponds to $R_{1\rho}$ of the water pool when there is no exchange and reads:

$$R_{\text{eff}} = R_{1a}\cos^2\theta + R_{2a}\sin^2\theta \quad [3]$$

This rate arises from the relaxation caused by direct water saturation and is the origin of the spillover effect. If a symmetric MT is also apparent, R_{eff} can be extended (32,34) by an exchange relaxation for MT to $R_{\mathrm{eff}}=R_{1\mathrm{a}}\cos^2\theta+R_{2\mathrm{a}}\cos^2\theta+R_{\mathrm{ex}}^{\mathrm{MT}}$. As we remove R_{eff} in the following, the exact knowledge of $R_{2\mathrm{a}}$ or $R_{\mathrm{ex}}^{\mathrm{MT}}$ is not important, as long as we have a reference value with the same R_{eff}. In agar phantoms, R_{eff} stays symmetric in Δω and the opposite frequency can be used. *In vivo*, the baseline can be estimated e.g. by a three-point method [Equation [21]].

The exchange weighting in CEST-MRI is induced by the rate R_{ex}. Hence, an appropriate evaluation method must provide direct access to R_{ex}. R_{ex} can be approximated by (32):

$$R_{\mathrm{ex}}(\Delta\omega_{\mathrm{b}})=k_{\mathrm{b}}f_{\mathrm{b}}\cdot\alpha\frac{\frac{\Gamma^2}{4}}{\frac{\Gamma^2}{4}+\Delta\omega_{\mathrm{b}}^2} \quad [4]$$

where $\Delta\omega_{\mathrm{b}}$ is the frequency offset with respect to the CEST pool b. The labeling efficiency can be approximated by (32):

$$\alpha=\frac{\omega_1^2}{\omega_1^2+k_{\mathrm{b}}(k_{\mathrm{b}}+R_{2\mathrm{b}})} \quad [5]$$

R_{ex} is a Lorentzian function of $\Delta\omega_{\mathrm{b}}$ with its maximum at $\Delta\omega_{\mathrm{b}}=0$, and linewidth:

$$\Gamma=2\sqrt{\frac{k_{\mathrm{b}}+R_{2\mathrm{b}}}{k_{\mathrm{b}}}\omega_1^2+(k_{\mathrm{b}}+R_{2\mathrm{b}})^2} \quad [6]$$

A useful quantity is the asymmetric MTR ($\mathrm{MTR}_{\mathrm{asym}}$), which attempts to isolate the contributions of CEST effects to the *Z* spectra using a reference scan without CEST effects, which can be the scan at opposite frequency or the fit of direct water saturation (23,24).

For agar phantoms, we use the opposite frequency signal as a reference. To abbreviate the following relations, we define the label scan around the resonance of pool b as $Z_{\mathrm{lab}} = Z(+\Delta\omega)$ and the reference scan at the opposite frequency with respect to water as $Z_{\mathrm{ref}} = Z(-\Delta\omega)$. For $Z_{\mathrm{ref}} = Z(-\Delta\omega)$, the effective relaxation $R_{\mathrm{eff}}(-\Delta\omega)$ is unchanged, i.e. $R_{\mathrm{eff}}(-\Delta\omega) = R_{\mathrm{eff}}(\Delta\omega)$. Hence, R_{ex} is only important for the labeling scan and R_{ex} can be neglected for the opposite frequency. Thus, the opposite frequency can be used as a reference scan $Z_{\mathrm{ref}} = Z(-\Delta\omega)$. [This reasoning assumes that: (i) R_{eff} is symmetric and no MT asymmetry or additional exchanging pools at $-\Delta\omega$ are present; and (ii) the width Γ of R_{ex} ($\Delta\omega_{\mathrm{b}}$) is smaller than the chemical shift ($\Gamma < \delta_{\mathrm{b}}$) of the corresponding pool.]

For cw steady-state CEST, it has been shown previously (32) that there are different MTR normalizations possible. The most common is the subtraction of the *Z*-values of the label and reference scan, giving the asymmetry of the *Z*-spectrum:

$$\mathrm{MTR}_{\mathrm{asym}}=Z_{\mathrm{ref}}-Z_{\mathrm{lab}}=\cos^2\theta\frac{R_{\mathrm{ex}}R_{1\mathrm{a}}}{R_{\mathrm{eff}}(R_{\mathrm{eff}}+R_{\mathrm{ex}})} \quad [7]$$

A reported spillover-corrected evaluation proposed by Liu *et al*. (35,36) normalizes with the reference value:

$$\mathrm{MTR}_{\mathrm{normref}}=\frac{Z_{\mathrm{ref}}-Z_{\mathrm{lab}}}{Z_{\mathrm{ref}}}=\frac{R_{\mathrm{ex}}}{R_{\mathrm{eff}}+R_{\mathrm{ex}}} \quad [8]$$

A probabilistic combined model (pcm) for *Z*-spectra, able to separate CEST from spillover and MT, of Zaiss *et al*. (22) can also be written as an MTR:

$$\mathrm{MTR}_{\mathrm{pcm}}=\frac{Z_{\mathrm{ref}}-Z_{\mathrm{lab}}}{Z_{\mathrm{ref}}-Z_{\mathrm{lab}}+Z_{\mathrm{lab}}Z_{\mathrm{ref}}}=\frac{R_{\mathrm{ex}}}{\cos^2\theta\cdot R_{1\mathrm{a}}+R_{\mathrm{ex}}} \quad [9]$$

This evaluation easily leads to the ideal proton transfer rate (PTR) = $k_a/(k_a + R_{1a})$ (1,37). However, the straightforward way to separate for R_{ex} is by subtraction of the inverse *Z*-values:

$$\mathrm{MTR}_{R\mathrm{ex}}=\frac{1}{Z_{\mathrm{lab}}}-\frac{1}{Z_{\mathrm{ref}}}=\frac{R_{\mathrm{ex}}}{\cos^2\theta\cdot R_{1\mathrm{a}}} \quad [10]$$

$\mathrm{MTR}_{\mathrm{asym}}$ contains a quadratic term of R_{eff} and $\mathrm{MTR}_{\mathrm{normref}}$ contains a linear term of R_{eff} in the denominator, while $\mathrm{MTR}_{\mathrm{pcm}}$ and $\mathrm{MTR}_{R\mathrm{ex}}$ are free of R_{eff} terms and therefore particularly free of R_{2a} and symmetric MT contributions.

The *Z*-spectrum and useful MTRs for pulsed-CEST

The assumption of $R_{1\rho}$ decay during the pulse (pulse duration t_p) and R_{1a} recovery during RF off (interpulse delay time t_d) leads to the following formula for the steady state in a pulsed SL experiment (30):

$$Z^{\mathrm{ss}}_{\mathrm{pulsed}}(\Delta\omega)=\frac{\left(1-\mathrm{e}^{-R_{1\mathrm{a}}\cdot t_{\mathrm{d}}}\right)-\frac{R_{1\mathrm{a}}\cdot\cos\theta}{R_{1\rho}(\Delta\omega)}\left(1-\mathrm{e}^{R_{1\rho}(\Delta\omega)\cdot t_{\mathrm{p}}}\right)}{\mathrm{e}^{R_{1\rho}(\Delta\omega)\cdot t_{\mathrm{p}}}-\mathrm{e}^{-R_{1\mathrm{a}}\cdot t_{\mathrm{d}}}} \quad [11]$$

This is the result of Santyr *et al*. (30) in our notation. Assuming small arguments of the exponential functions, we employ $\exp(x) \approx 1 + x$ and obtain – with the duty cycle (DC) = $t_p/(t_p + t_d)$ – an expression for the normalized steady–state magnetization Z^{ss} which is similar to the result for the cw case:

$$Z^{\mathrm{ss}}_{\mathrm{pulsed}}(\Delta\omega)\approx\frac{R_{1\mathrm{a}}(1-\mathrm{DC}+\cos\theta\cdot\mathrm{DC})}{R^{\mathrm{pulsed}}_{1\rho}(\Delta\omega)} \quad [12]$$

where:

$$R^{\mathrm{pulsed}}_{1\rho}(\Delta\omega)=R_{1\rho}(\Delta\omega)\cdot\mathrm{DC}+R_{1\mathrm{a}}\cdot(1-\mathrm{DC}) \quad [13]$$

Assuming cos θ = 1 and employing Equations [12] and [13] for $\mathrm{MTR}_{\mathrm{pcm}}$ [Equation [9]] and $\mathrm{MTR}_{R\mathrm{ex}}$ [Equation [10]] leads to the pulsed MTRs:

$$\mathrm{MTR}_{\mathrm{pcm}}=\frac{R_{\mathrm{ex}}\cdot \mathrm{DC}}{R_{1\mathrm{a}}+R_{\mathrm{ex}}\cdot \mathrm{DC}} \quad [14]$$

$$\mathrm{MTR}_{Rex}=\frac{R_{\mathrm{ex}}\cdot \mathrm{DC}}{R_{1\mathrm{a}}} \quad [15]$$

Therefore, the pulsed MTRs are only altered by the DC as a prefactor of R_{ex} against the cw case [cf. Equations [9] and [10]]. Thus, these spillover and MT corrections are likewise applicable to pulsed CEST.

Quantitative parameter determination

Equation [10] [with the expected parameter dependences as described in Equation [15]] provides a robust measure for qualitative contrast that avoids the effects from direct water saturation and exchange from symmetric macromolecular MT effects, and is hence superior to the current standard MTR_{asym}. However, ideally we would like a metric that quantitatively reports on a fundamental sample parameter. To extend this spillover correction method to a quantification method, we define the apparent exchange-dependent relaxation (AREX):

$$\mathrm{AREX}=\mathrm{MTR}_{Rex}R_{1\mathrm{a}} \quad [16]$$

AREX should yield $R_{ex}\cdot$ DC, which is given by DC, by Equation [4], and the labeling efficiency α [Equation [5]]. We can assume the maximum labeling efficiency ($\alpha \approx 1$) as long as the conditions $k_b << \omega_1$ and $R_{2b} << \omega_1$ hold [Equation [5]]. In this full-saturation limit, when applying irradiation at the b-pool resonance, $R_{ex} = k_b f_b = k_a$ [Equations [7] and [12]] and hence:

$$\mathrm{AREX}=k_{\mathrm{a}}\cdot \mathrm{DC} \quad [17]$$

Instead of modeling a pulse train by an average B_1 power, we now obtain a DC weighting of an average R_{ex} during the pulse. The implicit assumption that the average $R_{1\rho}$ during the pulse equals the cw relaxation rate is discussed below.

In summary, two conditions must be valid for AREX/DC = k_a: First, the full–saturation limit $\omega_1 >> k_b$ and, second, R_{2b} and the peak width [Equation [6]] must be smaller than the chemical shift difference to water ($\Gamma < \delta_b$). Considering amide protons of proteins at B_0 = 3 T, the CEST pool parameters are $k_b \sim 30\ s^{-1}$ and δ_b = 3.5 ppm (=447·2π s^{-1}) (1,4). As a model for amide exchange, we employ amine protons of creatine at lower pH (6.2–6.6) to obtain a comparable exchange rate ($k_b \sim 30$–$60\ s^{-1}$) (19). The smaller chemical shift δ_b = 1.9 ppm (=242·2π s^{-1}) challenges our method for spillover correction and is therefore a crucial test. For 1 μT < B_1 < 5 μT, both conditions are well fulfilled for creatine amine and amide protons:

$$k_{\mathrm{b}}=50\mathrm{s}^{-1}<<\omega_1=\frac{B_1}{\mu\mathrm{T}}\cdot 42.6\cdot 2\pi\mathrm{s}^{-1}\cong\frac{\Gamma}{2}<\frac{\delta_{\mathrm{b}}}{2}=121\cdot 2\pi\mathrm{s}^{-1}$$

In general, if peaks are broad and other pools ‘c’ are involved, the reference scan is also contaminated by non-zero exchange-dependent relaxation terms $R_{ex.ref} = R_{ex}(-\Delta\omega)$ in addition to the on-resonant term $R_{ex.lab} = R_{ex}(\Delta\omega)$. Thus, AREX yields:

$$\mathrm{AREX}=R^{\mathrm{b}}_{\mathrm{ex,lab}}-R^{\mathrm{b}}_{\mathrm{ex,ref}}+R^{\mathrm{c}}_{\mathrm{ex,lab}}-R^{\mathrm{c}}_{\mathrm{ex,ref}} \quad [18]$$

instead of $R_{ex,lab}$. Although affected by pool c and therefore no longer being selective, the resulting MTR_{Rex} is still free from symmetric spillover effects, and hence an apparent R_{ex} (AREX), which is still a pure exchange-dependent parameter.

pH mapping

Under the assumption of full saturation, AREX/DC is given by $k_b f_b$. Therefore, AREX of APT can be used to calculate the exchange rate by the formula previously derived by Sun *et al*. (38):

$$\mathrm{pH}(in\ vivo)=6.4+\log_{10}\left(\frac{\mathrm{AREX/DC}}{f_{\mathrm{b}}\cdot 5.57}\right) \quad [19]$$

For APT, f_b = 1 : 867 has been reported (38). For amine exchange of creatine, the k(pH) dependence was given by Goerke *et al*. (39). It can be rearranged to yield the absolute pH employing an AREX map:

$$\mathrm{pH}(19^{\circ}\mathrm{C})=\log_{10}\left(\frac{\mathrm{AREX/DC}}{f_{\mathrm{b}}\cdot 1.4615}\right) \quad [20]$$

A flow chart of how the theory and evaluation methods are applied to the raw data is given in Fig. 1.

METHODS

The proposed spillover correction based on the inverse metric was tested in CEST experiments with creatine model solutions at B_0 = 3 T, as well as with *in vivo* rat measurements at 9.4 T.

Phantoms

Eleven phantoms containing phosphorus-based sodium–potassium buffer at different pH values were measured. A transverse image is shown in Fig. 2 and their properties are listed in Table 1. Creatine monohydrate (Sigma–Aldrich, Steinheim, Germany) of 55.5mM concentration was added to each 50–mL tube. Two tubes had different creatine concentrations: F1, (2/3) × 55.5mM; F2, (1/3) × 55.5mM.

To vary the conditions for spillover and MT, 0.2–1% agar was added to a 55.5mM creatine solution at pH 6.38 (A1–A5, ‘solidified phantoms’). The pH value did not change during the heating process and addition of agar. Phantom 0 contained no agar, and PH1–PH3 were controls with different pH values of 6.2, 6.3 and 6.6, respectively.

Phantom parameters were estimated for a two-pool model by a full numerical fit of the Z spectra obtained for different RF amplitudes B_1 simultaneously, similar to the Quantification-of-exchange-by-saturation-power-method (QUESP) of McMahon *et al.* (40).

In vitro MRI experiments

Phantom imaging was performed on a 3-T whole-body MR scanner (Magnetom TIM-TRIO; Siemens, Erlangen, Germany). Z-spectra were obtained after saturation by a train of 80 Gaussian-shaped pulses with a duration t_p = 100 ms for each pulse and an interpulse delay t_d = 100 ms (DC = 50%) at B_1 = flip angle/(γt_p) = 0.2–2 μT, followed by single-shot turbo spin echo imaging (field of view, 220mm^2; matrix, 192 × 192; in-plane resolution, 1.1 × 1.1 × 4mm^3). Z-spectra were B_0 corrected employing a water saturation shift referencing (WASSR) map (41). After B_0 correction, the MTRs according to Equations [7], [8], [9] and [10] were calculated pixel by pixel and by region of interest (ROI) evaluation, employing the opposite frequency as reference scan Z_{ref}. MTR$_{Rex}$ was compared with analytical R_{ex} and k_a values determined by the numerical fit. Fitting of Z-spectra was performed by stepwise matrix solution (33) of the two-pool Bloch–McConnell equations.

T_1-weighted MR images were acquired by a saturation recovery gradient echo sequence (TE = 4ms; TR = 8ms; 4 shots; 4 averages; field of view, 220mm^2; matrix, 256 × 256; in-plane resolution, 0.9× 0.9 × 4 mm^3; flip angle, 8°). Altogether, 21 contrasts at different recovery times between 50ms and 5 s were fitted to obtain T_1 maps.

T_2-weighted MR images were acquired by a spin echo sequence with 32 echo delays (TE = 11–352ms; TR= 6 s; field of view, 220 mm^2; matrix, 192 × 192; in-plane resolution, 1.1× 1.1× 4 mm^3; flip angle, 180°). A pixel-by-pixel logarithmic fit was applied to obtain T_2 maps.

Animal preparation

All animal-related procedures were approved by the Institutional Animal Care and Use Committee at Vanderbilt University. The middle cerebral artery occlusion model was adapted on spontaneously hypertensive male rats (Charles Rivers Laboratory, Wilmington, MA, USA) weighing between 275 and 300 g, as described previously (42). Specifically, rats were anesthetized with isoflurane (3% for induction and 2% during surgery) via a vaporizer with O_2. A midline neck incision was made and the common, external and internal carotid arteries were identified on the right side and isolated from the surrounding structures. The proximal branches of the external carotid artery were ligated and an arteriotomy was made in the external carotid artery. A 0.37-mm-diameter silicon-coated 4–0 nylon suture (Doccol Corporation, Redlands, CA, USA) was introduced into the vessel and routed into the internal carotid artery. The suture was pushed into the internal carotid artery until a mild resistance was felt and the middle cerebral artery was occluded (at a length of 18–20 mm) and the suture was left there. The body temperature was maintained with a heating pad during surgery. The wound was then closed and buprenorphine was administered for post-operative pain management.

In vivo MRI experiments

Animal imaging was performed 48 h after surgery on a 9.4-T horizontal MRI scanner (Varian, Palo Alto, CA, USA). Bite and head bars were used to secure the animal during imaging to reduce respiration-induced motion artifacts. The rectal temperature was kept at 37 °C using a warming air feedback system. Single-shot echo planar imaging was used for acquisition and a triple-reference imaging scheme (43) was used to reduce echo planar imaging artifacts. Measurement parameters were: matrix size, 64; TE = 28 ms. Pulse train parameters were: t_p = 12.5 ms; B_1 = 0.84 μT; DC = 50%; flip angle, 180°; n = 200.

Evaluation

The opposite frequency is a reasonable choice for the reference scan [$Z_{ref} = Z(-3.5\ \text{ppm})$] for the phantom study. However, in *in vivo Z* spectra, the opposite side is contaminated by MT and peaks caused by nuclear Overhauser effects.

Therefore, for the *in vivo* APT signal, the three-point method proposed by Jin *et al*. (44) was employed on a pixel-by-pixel basis. Using the same Z_{ref}:

$$z^*_{\text{ref}} = \frac{Z(3.0\text{ppm}) + Z(4.2\text{ppm})}{2}; Z_{\text{lab}} = Z(3.5\text{ppm}) \quad [21]$$

we define the spillover- and MT-corrected parameter MTR_{Rex}:

$$\text{MTR}^*_{Rex} = 1/Z_{\text{lab}} - 1/Z^*_{\text{ref}} \quad [22]$$

and, according to Equation [16], also the T_1 relaxation-compensated parameter AREX*. To enhance sensitivity for ROI evaluations, the MTR values of 3.4, 3.5 and 3.6ppm were averaged using Z_{ref} from a linear interpolation of the points at 3 and 4.2 ppm.

RESULTS

This section is divided into three parts. First, we present the outcome of *Z*-spectroscopy of the solidified phantoms and how the different metrics allow for spillover correction. Second, we show the quantitative metric AREX and how the exchange rate and pH mapping can be obtained after compensation for effects of T_1 relaxation. Third, the metrics are applied to *in vivo* data of stroke in rat brain.

Spillover correction

Figure 3a shows distinct effects in the *Z*-spectrum on addition of 1% agar (phantom A5) in experiments at B_0 = 3 T. The corresponding asymmetry is strongly diluted compared with the creatine solution without agar (phantom 0) (MTR_{asym}, Fig. 3b). Even in the case of full saturation of the CEST pool (B_1 > 1 μT), we still observe a strong dependence of MTR_{asym} on B_1 in the solidified phantom. $\text{MTR}_{normref}$ (Fig. 3c) provides an enhancement of the signal of the solidified phantom, but displays an underestimation of the CEST effect by about 30% and a strong dependence on the amplitude B_1 of the saturating field. Both MTR_{pcm} and MTR_{Rex} give very similar values for solidified and non-solidified phantoms. This can be seen not only in the case of on-resonant irradiation on pool b, but also the shape of the CEST

peak is coherent with the peak of the control measurement in the absence of agar. This proves the validity of our spillover correction for arbitrary frequency offsets. In the case of full saturation, the dependence of MTR_{Rex} and MTR_{pcm} on B_1 is less than 15%, producing a small overestimation of the effect. Near the center of the water proton resonance at 0 ppm, all MTRs show considerable deviations, which are even larger for the inverse MTR_{pcm} and MTR_{Rex}. Errors increase tremendously, which is discussed in detail below (Fig. 10).

Images of MTR_{asym} and MTR_{Rex} at 1.83 ppm display the same relation: Spillover is not critical for small B_1, whereas, for stronger B_1, spillover dilutes MTR_{asym} significantly. In contrast, MTR_{Rex} yields a homogeneous contrast up to B_1 = 1.4 μT independent of the agar concentration (Fig. 4). Figure 4 demonstrates the importance of spillover correction, as MTR_{asym} causes the misinterpretation of diluted signals as changes in pH or concentration. At B_1 = 2 μT, the agar tubes A2 and A3 show a very similar contrast as tube F2 in the presence of one-third of the creatine concentration. For exceedingly high B_1, the contrast-to-noise ratio (CNR) is insufficient and MTR_{Rex} cannot completely reconstruct the ideal signal from the residual signal. MTR_{Rex} also enhances the signals from the tubes without agar: different pH and different concentration can therefore be distinguished better after correction.

Figure 5 displays MTR as a function of B_1. Using MTR_{Rex} or MTR_{pcm}, the plateau of the full-saturation limit is reached, whereas MTR_{asym} and $MTR_{normref}$ show the known decrease in the CEST effect caused by spillover dilution induced by MT, T_2 relaxation and B_1. Thus, in the full-saturation limit, a spillover correction is also a first-order B_1 correction.

Quantification

The numerical Bloch–McConnell fit of ROI-averaged Z spectra for different B_1 values yields the characterization of the phantom parameters listed in Table 1. The values for the exchange rates k_b agree well with water exchange spectroscopy (WEX) data measured by Goerke *et al*. (39). The relative concentrations f_b are in good agreement with the prepared creatine concentration if the number of exchanging protons per molecule is 4. R_{2b} values are quite constant at approximately 50 s^{-1}, which is comparable with the exchange rate.

MTR_{Rex} and MTR_{pcm} were calculated using B_1, DC, k_b, f_b, R_{1a}, R_{2b} and the formula for the rate R_{ex} [Equation [4]].

The pulsed approach of Santyr *et al*. (30) is known to deviate, especially for slow exchange rates (45). Roeloffs *et al*. (45) showed that a biexponential decay during the break must be modeled to properly extend the model of Santyr *et al*. (30). For spillover and MT correction, we believe that this is not important as the deviation is still only exchange dependent; for quantification, however, this may have an influence. Nevertheless, the comparison of MTR_{Rex} calculated from fitting results with MTR_{Rex} obtained from the data (Fig. 5) shows that the corrected curves can still be interpreted by the analytical solution for MTR_{Rex} [Equations [10] and [15]] based on the model of Santyr *et al*. (30). We believe that, because we used 100-ms Gaussian pulses, which end with a low power, the equilibrium between pool a and pool b is not changed greatly directly after the pulse, making the biexponential decay less important. However, this should be studied in detail and may limit our approach

for pulsed CEST of slow exchanging systems saturated with different pulse shapes. However, with our pulse parameters, the step from spillover-corrected MTR_{Rex} to a reliable quantification of the back exchange rate k_a is straightforward by employing Equation [17] (Fig. 6). AREX is therefore proportional to the concentration f_b and the exchange rate k_b. It varies between phantoms F1, F2 and 0, and also between phantoms 0, PH1, PH2 and PH3. AREX yields homogeneous contrast in phantoms 0 and A1–A5. However, a small overestimation of k_a in the agar phantoms compared with the control (0) is observed.

Using the exchange rate of creatine protons, k_b(pH 6.38, T= 19 °C) = 35 s^{-1}, measured in WEX experiments (39), a map of the relative proton fraction f_b can be obtained which is valid for the given pH and is in agreement with the fitted results. Together with the prepared creatine concentration (55.5m$_M$), this approach yields the number of labile protons per creatine molecule, $N = f_b \times [2H_2O]/[Cr]$. For pH ≤ 6.4, N is most probably 4, in conformity with the zwitterionic structure of creatine (Fig. 2b) and the pK_a value of the creatine amine groups (pK_a = 6.6 at T = 37 °C) (5). For the phantom at pH 6.6, the proton number might be smaller. Assuming four exchanging amine protons for creatine, the value of f_b can be derived for any creatine concentration. Together with k_a = AREX/DC, we obtain a k_b map. Finally, using the dependence of the creatine amine exchange rate k_b on pH found by Goerke *et al*. (39), a map of absolute pH values can be calculated. The resulting data are in good agreement with pH values prepared in the phantoms (Fig. 6). This proves that spillover, MT and T_1 relaxation compensation worked well for the creatine–agar phantoms.

Application *in vivo*

Having demonstrated the validity of the introduced corrections, the formalism can be applied to *in vivo* data. In a stroke lesion of rat brain, we expect a drop in APT because of the pH drop, which is clearly visible in Fig. 7. The *Z*-spectrum at 3.5 ppm is contaminated by direct saturation and MT effects (Fig. 7d, g); therefore, the baseline estimation of Jin *et al*. (44) was employed as a reference. After correction of spillover by MTR_{Rex}, the CNR between normal and lesion tissue increases from CNR = 1.17 to CNR = 1.44 (values correspond to ROIs in Fig. 8). In addition, the T_1 map (Fig. 7e) shows a difference between lesion and healthy tissue (Fig. 7b). This can be corrected by the AREX evaluation, showing an even higher CNR = 1.62 between normal and pathologic tissue (Fig. 7c). It should be noted that the delay time and rotation transfer effects were taken into account using DC = 1 to calculate k_a. Finally, employing Equation [19] and the reported proton fraction f_b = 0.115%, an absolute pH map can be calculated from AREX. It shows pH values between 7 and 7.2 in normal tissue and a drop to around 6.5 within the lesion (Fig. 7f).

A further check of the spillover correction is possible by investigating the behavior with increasing B_1, which is shown for the phantoms in Fig. 4. A similar signature in the MTRs as a function of B_1 was observed after spillover correction of ROI-averaged data (Fig. 8b, c): For low B_1, APT*, MTR_{Rex}* and AREX* show an increase with B_1. After reaching a maximum at 1.6 μT, the signals drop again. However, the decrease for the spillover-corrected methods is less significant and a type of plateau is reached. Again, the APT contrast after spillover correction is shown to be less B_1 dependent. It is important to note the increase in contrast between tissue in the lesion and normal tissue. For AREX, the

contrast difference is much larger than the standard deviation. Therefore, AREX leads to a purer but also larger contrast.

DISCUSSION

In this study, we have shown that MTR_{Rex}, employing the inverse metric of the *Z*-spectrum, enables the removal of spillover and MT effects from CEST signals.

As depicted in Fig. 1, only simple mathematical operations are needed to obtain a spillover-corrected signal from raw *Z*-spectra data. Previous studies on spillover by Sun *et al*. (19,20,46) treated the spillover effect by introducing a spillover coefficient σ of the ideal MTR, i.e. $MTR_{real} = (1 - \sigma)\alpha MTR_{ideal}$ [α is the labeling efficiency, Equation [5]]. In contrast with this approach, we observed that spillover dilution can be better explained by the inverse addition of contributing effects. Spillover dilution of a CEST effect induced by 'parallel' saturation of water resembles the 'dilution' of a resistor R_b by a parallel circuit to another resistor R_a. If the diluted resistance R_{a+b} and the resistance of R_a are known, we obtain $1/R_b = (1/R_{a+b}) - (1/R_a)$.

The reason why superposition and not inverse superposition of effects in the *Z*-spectrum was also successful in other treatments originates from the approximation $Z = 1/(1 + x) \approx (1 - x)$ valid for $R_{eff} \approx R_{1a}$ and small $x \approx R_{ex}/R_{1a}$. This is also the principal reason why superpositions of Lorentzians can be fitted to steady-state pulsed CEST spectra. According to our results, a superposition of reciprocal Lorentzians should be more suitable. The observation that $1/Z$ yields basically a $R_{1\rho}$ spectrum [Equation [1]] further supports the importance of the inverse *Z*-spectrum. $R_{1\rho}$, known from SL experiments, has, as a relaxation rate, the property of being a superposition of the apparent exchange-dependent relaxation effects [Equation [2] (34)].

Some degree of dilution was identified as a spillover effect by Sun *et al*. (19,20,46). In our approach, this contribution is regarded as a loss in labeling efficiency. The latter can be defined more generally as $\alpha = R_{ex}/k_a$, yielding (29):

$$\alpha = \frac{\frac{(\omega_b-\omega_a)^2}{\omega_1^2+\Delta\omega^2}k_b+R_{2b}}{\underbrace{k_b+R_{2b}}_{*}}\frac{\omega_1^2}{\omega_1^2+k_b(k_b+R_{2b})} \quad [23]$$

A comparison of Equation [23] with α of Equation [5], which is similar to α given in ref. (37), reveals an additional factor (*) in Equation [23], which decreases with increasing B_1. This factor is maximal at $\Delta\omega = 0$ and can be interpreted as the on-resonance effects induced by the exchange. These effects are employed in on-resonant SL experiments. The loss of labeling is attributed to an interference of off-resonant and on-resonant features of R_{ex}. Hence, the labeling efficiency is a useful parameter which was extended by the eigenspace approach (29), whereas a spillover coefficient is not appropriate to the inverse metric.

Other than the spillover correction employed by Sun *et al*. (19) and the 'isolation' of R_{ex} from $R_{1\rho}$ ($R_{ex} = R_{1\rho} - R_{eff}$) proposed by Jin *et al*. (14), which both use additional T_2 and B_1 mapping, our approach employs only the intrinsic metric to correct spillover. This is

advantageous because it reduces the scanning time and post-processing efforts. The intrinsic structure was employed in a similar manner in the fitted model of ref. (22) which is the origin of MTR_{pcm} [Equation [5]].

It is important to note that the isolation and correction of effects are different operations. Although the former approaches, such as MTR_{asym}, isolate signals from specific effects, these isolated effects can still be diluted (Fig. 3). Therefore, removing the information about parallel effects must be considered carefully, as other contributions may become invisible, but can still be effective as dilutions.

The approach of Liu *et al*. (35) [Equation [8]] afforded a partial spillover correction which could be explained by the reduction of the quadratic term of R_{eff} in MTR_{asym} to a linear one. Their normalization is considered to be appropriate for glutamate-CEST imaging (7,47) and glycosaminoglycan-CEST (48). In particular, these two applications can also benefit from the improvement of the MTR_{Rex} evaluation.

Next, we discuss our quantitative approach. To the best of our knowledge, there are two different approaches to model the pulsed CEST case: (i) using cw theory with an equivalent cw power (12,49) verified to be valid for slow exchange rates by Tee *et al*. (50); (ii) the approach of Santyr *et al*. (30) for SL, which should also be valid for CEST by relying on the equivalence of SL and CEST (29). The SL solution of Santyr *et al*. (30) takes into account different relaxation during and between the pulses. However, Santyr *et al*. (30) assume solely a monoexponential decay in the interpulse delay, which cannot explain the modulations as a function of the flip angle observed by CERT (28) or the dependence on the delay time (51). However, for long pulses, as employed in this study, our results suggest that the approach of Santyr *et al*. (30) is also valid for pulsed CEST. We did not observe a perfect match of the theory of Santyr *et al*. (30) and the corrected data, which we attribute to the invalid assumption of monoexponential dynamics in the interpulse delay and the assumption of full saturation ($R_{ex} = k_a$) during the Gaussian pulse. R_{ex} obtained by AREX is therefore an effective parameter which incorporates the dependence on pulse shape, as well as processes occurring between the pulses.

The inverse metric is valid only for pulsed CEST/SL if $R_{1\rho}t_p << 1$ [assumption of Equation [12]], which is not the case for large R_2 and θ or t_p. This could explain why the agar phantoms show slightly different MTR_{Rex} compared with the solutions without agar (Fig. 4). In principle, this limits the inverse approach to applications with pulses that are much shorter or much longer than $1/R_{1\rho}(\Delta\omega)$. The latter corresponds to the cw case. In practice, *Z*-values are directly tunable by B_1 and can be set to values that are not smaller than 0.5; then, $R_{1\rho} \sim 2R_{1a}$ and the condition $R_{1\rho}t_p << 1$ is easier to fulfill.

Pulsed CEST including MT was also studied with similar phantom parameters by Desmond and Stanisz (18), who interpreted their data with numerical Bloch–McConnell simulations. With the addition of agar, T_2 is changed strongly. However, a limitation of our study is that MT was only shown to be corrected up to 1% agar, which corresponds to a fraction of about $f_b = 0.3\%$ (52). In contrast, fractions up to $f_b = 18\%$ are possible in cartilage (53). For cw simulations, it was shown that the inverse superposition is appropriate up to $f_b = 5\%$ (29),

but then the assumption of the simple superposition $R_{1\rho} = R_{\text{eff}} + R_{\text{ex,CEST}} + R_{\text{ex,MT}}$ might be invalid.

The intermediate exchange regime was not explicitly considered in this study. In this case, the spillover correction of MTR_{Rex} is promising, but still remains to be proven. Although demonstrated so far for amine and amide exchange, we expect that our normalization will work for diamagnetic and paramagnetic CEST in the slow and intermediate exchange regimes, and for the generation of qualitative contrast and quantitative parameter fittings.

Application in the case of non-steady-state and inversion pulses

For *in vivo* protocols, the saturation times are commonly kept shorter, in the range of one or two T_1, to save scanning time or avoid dominant spillover effects (6,7). In addition, more efficient inversion pulses are commonly used (23,24,49,51). Additional measurements in non-steady state with only 3-s irradiation ($\sim 1 \times T_1$) were performed (Fig. 9a, b, e), as well as saturation with a pulse train of 180° pulses (Fig. 9c, d, f), for the phantom described in Fig. 2. In both cases, the homogeneity between the agar phantoms was improved by the inverse evaluation MTR_{Rex} against MTR_{asym}. However, within each phantom, the inverse metric induced a less homogeneous contrast. From theory, it is known (32) that the inverse metric is not valid for the transient state. However, near steady state ($t_{\text{sat}} \approx T_1$), it can still be used as an approximation. For inversion transfer or CERT, there is no analytical knowledge, but our results indicate that the general *Z*-spectrum structure might also be similar for rotation transfer.

Systematic and statistical errors

Figure 10 depicts the increase in errors for MTR_{Rex}. If we turn to the $1/Z$ metric, the relative errors are similar, $\Delta(1/Z)/(1/Z) = \Delta Z/Z$, but the absolute errors increase, $\Delta(1/Z) = (1/Z^2)\Delta Z$. For example, $R_1 = 1\ \text{s}^{-1}$ and a dominant direct saturation at the label frequency of $R_{\text{eff}} = 2R_1$ leads to $Z = 0.5$. Hence, the statistical error of $1/Z$ is four times the error of Z.

However, MTR_{asym} also has a quadratic term of R_{eff} in the denominator; therefore, $\text{MTR}_{\text{asym}} \sim 1/Z^2 \cdot \text{PTR}$. Thus, the CEST effect estimated by MTR_{aysm} has a systematic error on the order of $1/Z^2$. This means, by the inverse metric, we trade systematic errors against statistical errors, which can be reduced by averaging. This also indicates that B_1 should not exceed a certain limit to keep Z and the signal-to-noise ratio large. For the estimation of the signal-to-noise ratio, MTR_{asym} is a good indicator.

Figure 8 indicates that a spillover correction is also a B_1 correction near the full-saturation limit ($\alpha \approx 1$). Although MTR_{asym} shows a strong dependence on B_1 and must be corrected by post-processing, as proposed by Sun *et al*. (46), MTR_{Rex} is almost constant up to $B_1 = 2$ μT. For faster exchange and partial saturation, the tissue-dependent B_1 correction of Singh *et al*. (54), reported at $B_0 = 7$ T, should be performed with spillover-corrected MTR_{Rex} instead of $\text{MTR}_{\text{normref}}$. We do not recommend the application of a B_1 correction to spillover-diluted data, but suggest that B_1 corrections should be applied directly to R_{ex}.

Imaging of stroke

In the rat CEST imaging study of Sun *et al*. (15), APT of normal tissue was reported to be 2.94%, whereas, in the lesion, it dropped to 0.9%. This was stronger than the signal decrease of about a factor of 0.5 observed in our animal study. In addition, in pH mapping, we only saw a drop of 0.5 pH units, whereas a pH decrease of approximately 1 pH unit was reported in ref. (15). In this and other studies (17,38), the correlation with lesions detected by diffusion and perfusion imaging was investigated. In our experiments, the resolution was too low to resolve significant substructures within the lesion. In contrast with other studies, we avoided contaminations of asymmetry analysis by employing a baseline estimation (44). We believe that this is beneficial, especially because significant nuclear Overhauser effects and shifted macromolecular MT effects are apparent in the brain parenchyma. It should be noted that this method can only be applied at higher fields ($B_0 \geq 7$ T). For lower B_0, we suggest a Lorentzian line fit of the water resonance as an appropriate reference.

CONCLUSION

We propose a new spillover and MT correction method for the evaluation of *Z*-spectra which requires no information about T_2 and MT of the system and is easily applied. The validity of the proposed corrected MTR (MTR_{Rex}) was demonstrated for an *in vitro* system, yielding high spillover, i.e. creatine, in agar gels at clinical field strengths. MTR_{Rex} was extended to a T_1 relaxation-compensated metric, called AREX (for ‘apparent exchange-dependent relaxation’), which allowed the quantitative evaluation of *Z*-spectra and could be verified by numerical fits. The validity, sensitivity and performance of the metric require sufficiently large *Z*-values ($Z>0.5$) and an appropriate reference scan. APT-CEST-MRI experiments of acute stroke in rat brain at B_0=9.4 T fulfilled these requirements. The outcome of the evaluation by means of the AREX metric was a significantly higher contrast between the stroke area and normal tissue compared with the contrast obtained using the non-inverse metric. Hence, we propose the application of the AREX metric for the analysis of *Z*-spectra data of all pathologies in which changes in MT, T_2 or T_1 are observed, in particular in tumors or tissue affected by stroke. With an appropriate reference scan, AREX may help to provide a pure exchange-dependent and exchange site-specific CEST contrast.

Abbreviations used

AREX	apparent exchange-dependent relaxation
APT	amide proton transfer
CEST	chemical exchange saturation transfer
CERT	chemical exchange rotation transfer
CNR	contrast-to-noise ratio
cw	continuous wave
DC	duty cycle
M_0	thermal equilibrium magnetization

MT	magnetization transfer
MTR	magnetization transfer ratio
MTR_{asym}	magnetization transfer ratio asymmetry
$MTR_{normref}$	magnetization transfer ratio normalized by reference scan
MTR_{pcm}	magnetization transfer ratio of probabilistic combined model
MTR_{Rex}	spillover-corrected magnetization transfer ratio yielding R_{ex}
$M_{z,sat}$	z magnetization after saturation
PTR	proton transfer rate
QUESP	Quantification of exchange by saturation power
R_{eff}	effective water relaxation in the rotating frame
R_{ex}	exchange-dependent relaxation in the rotating frame
ROI	region of interest
RF	radiofrequency
SL	spin-lock
WASSR	water saturation shift referencing.

REFERENCES

1. Zhou J, van Zijl PCM. Chemical exchange saturation transfer imaging and spectroscopy. Prog. Nucl. Magn. Reson. Spectrosc. 2006; 48(2–3):109–136.
2. van Zijl PCM, Yadav NN. Chemical exchange saturation transfer (CEST): what is in a name and what isn't? Magn. Reson. Med. 2011; 65(4):927–948. [PubMed: 21337419]
3. Terreno E, Castelli DD, Aime S. Encoding the frequency dependence in MRI contrast media: the emerging class of CEST agents. Contrast Media Mol. Imaging. 2010; 5(2):78–98. [PubMed: 20419761]
4. Zhou J, Payen J-F, Wilson DA, Traystman RJ, van Zijl PCM. Using the amide proton signals of intracellular proteins and peptides to detect pH effects in MRI. Nat. Med. 2003; 9(8):1085–1090. [PubMed: 12872167]
5. Haris M, Nanga RPR, Singh A, Cai K, Kogan F, Hariharan H, Reddy R. Exchange rates of creatine kinase metabolites: feasibility of imaging creatine by chemical exchange saturation transfer MRI. NMR Biomed. 2012; 25(11):1305–1309. [PubMed: 22431193]
6. Kogan F, Haris M, Singh A, Cai K, Debrosse C, Nanga RPR, Hariharan H, Reddy R. Method for high-resolution imaging of creatine in vivo using chemical exchange saturation transfer. Magn. Reson. Med. 2013
7. Cai K, Haris M, Singh A, Kogan F, Greenberg JH, Hariharan H, Detre JA, Reddy R. Magnetic resonance imaging of glutamate. Nat. Med. 2012; 18(2):302–306. [PubMed: 22270722]
8. Ling W, Regatte RR, Navon G, Jerschow A. Assessment of glycosaminoglycan concentration in vivo by chemical exchange-dependent saturation transfer (gagCEST). Proc. Natl. Acad. Sci. U. S. A. 2008; 105(7):2266–2270. [PubMed: 18268341]
9. Schmitt B, Zbýn S, Stelzeneder D, Jellus V, Paul D, Lauer L, Bachert P, Trattnig S. Cartilage quality assessment by using glycosaminoglycan chemical exchange saturation transfer and (23)Na MR imaging at 7 T. Radiology. 2011; 260(1):257–264. [PubMed: 21460030]

10. Singh A, Haris M, Cai K, Kassey VB, Kogan F, Reddy D, Hariharan H, Reddy R. Chemical exchange saturation transfer magnetic resonance imaging of human knee cartilage at 3 T and 7 T. Magn. Reson. Med. 2012; 68(2):588–594. [PubMed: 22213239]
11. Chan KWY, McMahon MT, Kato Y, Liu G, Bulte JWM, Bhujwalla ZM, Artemov D, van Zijl PCM. Natural D-glucose as a biodegradable MRI contrast agent for detecting cancer. Magn. Reson. Med. 2012; 68(6):1764–1773. [PubMed: 23074027]
12. Sun PZ, Benner T, Kumar A, Sorensen AG. Investigation of optimizing and translating pH-sensitive pulsed-chemical exchange saturation transfer (CEST) imaging to a 3 T clinical scanner. Magn. Reson. Med. 2008; 60(4):834–841. [PubMed: 18816867]
13. Longo D, Colombo S, Dastrù W, Poggi L, Tedoldi F, Terreno E, Uggeri F, Aime S. Evaluating iopamidol as pH-responsive CEST agent at 3 and 7 T. Contrast Media Mol. Imaging. 2009; 4(6): 294–295.
14. Jin T, Wang P, Zong X, Kim S-G. Magnetic resonance imaging of the Amine-Proton EXchange (APEX) dependent contrast. Neuroimage. 2012; 59(2):1218–1227. [PubMed: 21871570]
15. Sun PZ, Murata Y, Lu J, Wang X, Lo EH, Sorensen AG. Relaxation-compensated fast multislice amide proton transfer (APT) imaging of acute ischemic stroke. Magn. Reson. Med. 2008; 59(5): 1175–1182. [PubMed: 18429031]
16. Sun PZ, Zhou J, Huang J, van Zijl P. Simplified quantitative description of amide proton transfer (APT) imaging during acute ischemia. Magn. Reson. Med. 2007; 57(2):405–410. [PubMed: 17260362]
17. Sun PZ, Wang E, Cheung JS, Zhang X, Benner T, Sorensen AG. Simulation and optimization of pulsed radio frequency irradiation scheme for chemical exchange saturation transfer (CEST) MRI – demonstration of pH-weighted pulsed-amide proton CEST MRI in an animal model of acute cerebral ischemia. Magn. Reson. Med. 2011; 66(4):1042–1048. [PubMed: 21437977]
18. Desmond KL, Stanisz GJ. Understanding quantitative pulsed CEST in the presence of MT. Magn. Reson. Med. 2012; 67(4):979–990. [PubMed: 21858864]
19. Sun PZ, Sorensen AG. Imaging pH using the chemical exchange saturation transfer (CEST) MRI: correction of concomitant RF irradiation effects to quantify CEST MRI for chemical exchange rate and pH. Magn. Reson. Med. 2008; 60(2):390–397. [PubMed: 18666128]
20. Sun PZ, van Zijl PCM, Zhou J. Optimization of the irradiation power in chemical exchange dependent saturation transfer experiments. J. Magn. Reson. 2005; 175(2):193–200. [PubMed: 15893487]
21. Sun PZ. Simultaneous determination of labile proton concentration and exchange rate utilizing optimal RF power: radio frequency power (RFP) dependence of chemical exchange saturation transfer (CEST) MRI. J. Magn. Reson. 2010; 202(2):155–161. [PubMed: 19926319]
22. Zaiss M, Schmitt B, Bachert P. Quantitative separation of CEST effect from magnetization transfer and spillover effects by Lorentzian-line-fit analysis of z-spectra. J. Magn. Reson. 2011; 211(2): 149–155. [PubMed: 21641247]
23. Jones CK, Polders D, Hua J, Zhu H, Hoogduin HJ, Zhou J, Luijten P, van Zijl PCM. In vivo three-dimensional whole-brain pulsed steady-state chemical exchange saturation transfer at 7 T. Magn. Reson. Med. 2012; 67(6):1579–1589. [PubMed: 22083645]
24. Dula AN, Arlinghaus LR, Dortch RD, Dewey BE, Whisenant JG, Ayers GD, Yankeelov TE, Smith SA. Amide proton transfer imaging of the breast at 3 T: establishing reproducibility and possible feasibility assessing chemotherapy response. Magn. Reson. Med. 2013; 70(1):216–224. [PubMed: 22907893]
25. Lee J-S, Regatte RR, Jerschow A. Isolating chemical exchange saturation transfer contrast from magnetization transfer asymmetry under two-frequency rf irradiation. J. Magn. Reson. 2012; 215(0):56–63. [PubMed: 22237631]
26. Scheidegger R, Vinogradov E, Alsop DC. Amide proton transfer imaging with improved robustness to magnetic field inhomogeneity and magnetization transfer asymmetry using Saturation with Frequency Alternating RF Irradiation (SAFARI). Magn. Reson. Med. 2011; 66(5): 1275–1285. [PubMed: 21608029]

27. Zu Z, Janve VA, Li K, Does MD, Gore JC, Gochberg DF. Multi-angle ratiometric approach to measure chemical exchange in amide proton transfer imaging. Magn. Reson. Med. 2012; 68(3): 711–719. [PubMed: 22161770]
28. Zu Z, Janve VA, Xu J, Does MD, Gore JC, Gochberg DF. A new method for detecting exchanging amide protons using chemical exchange rotation transfer. Magn. Reson. Med. 2013; 69(3):637–647. [PubMed: 22505325]
29. Zaiss M, Bachert P. Equivalence of spin-lock and magnetization transfer NMR experiments. arXiv: 12032067 [Internet]. Available at: http://arxiv.org/abs/1203.2067.
30. Santyr GE, Fairbanks EJ, Kelcz F, Sorenson JA. Off-resonance spin locking for MR imaging. Magn. Reson. Med. 1994; 32(1):43–51. [PubMed: 8084236]
31. Zaiss M, Schnurr M, Bachert P. Analytical solution for the depolarization of hyperpolarized nuclei by chemical exchange saturation transfer between free and encapsulated xenon (HyperCEST). J. Chem. Phys. 2012; 136(14):144106. [PubMed: 22502500]
32. Zaiss M, Bachert P. Exchange-dependent relaxation in the rotating frame for slow and intermediate exchange – modeling off-resonant spin-lock and chemical exchange saturation transfer. NMR Biomed. 2013; 26(5):507–518. [PubMed: 23281186]
33. Woessner DE, Zhang S, Merritt ME, Sherry AD. Numerical solution of the Bloch equations provides insights into the optimum design of PARACEST agents for MRI. Magn. Reson. Med. 2005; 53(4):790–799. [PubMed: 15799055]
34. Trott O, Palmer AG 3rd. Theoretical study of R(1rho) rotating-frame and R2 free-precession relaxation in the presence of n-site chemical exchange. J. Magn. Reson. 2004; 170(1):104–112. [PubMed: 15324763]
35. Liu G, Gilad AA, Bulte JWM, van Zijl PCM, McMahon MT. High-throughput screening of chemical exchange saturation transfer MR contrast agents. Contrast Media Mol. Imaging. 2010; 5(3):162–170. [PubMed: 20586030]
36. Liu G, Song X, Chan KWY, McMahon MT. Nuts and bolts of chemical exchange saturation transfer MRI. NMR Biomed. 2013; 26(7):386–391. [PubMed: 23045158]
37. Zhou J, Wilson DA, Sun PZ, Klaus JA, van Zijl PCM. Quantitative description of proton exchange processes between water and endogenous and exogenous agents for WEX, CEST, and APT experiments. Magn. Reson. Med. 2004; 51(5):945–952. [PubMed: 15122676]
38. Sun PZ, Wang E, Cheung JS. Imaging acute ischemic tissue acidosis with pH-sensitive endogenous amide proton transfer (APT) MRI – correction of tissue relaxation and concomitant RF irradiation effects toward mapping quantitative cerebral tissue pH. Neuroimage. 2012; 60(1): 1–6. [PubMed: 22178815]
39. Goerke, S.; Zaiss, M.; Bachert, P. Water Exchange (WEX) spectroscopy on creatine model solutions; Proceedings of the 29th Annual Scientific Meeting ESMRMB; Lisbon, Portugal. 2012. p. 394
40. McMahon MT, Gilad AA, Zhou J, Sun PZ, Bulte JWM, van Zijl PCM. Quantifying exchange rates in chemical exchange saturation transfer agents using the saturation time and saturation power dependencies of the magnetization transfer effect on the magnetic resonance imaging signal (QUEST and QUESP): pH calibration for poly-L-lysine and a starburst dendrimer. Magn. Reson. Med. 2006; 55(4):836–847. [PubMed: 16506187]
41. Kim M, Gillen J, Landman BA, Zhou J, van Zijl PCM. Water saturation shift referencing (WASSR) for chemical exchange saturation transfer (CEST) experiments. Magn. Reson. Med. 2009; 61(6):1441–1450. [PubMed: 19358232]
42. Liu K, Mori S, Takahashi HK, Tomono Y, Wake H, Kanke T, Sato Y, Hiraga N, Adachi N, Yoshino T, Nishibori M. Anti-high mobility group box 1 monoclonal antibody ameliorates brain infarction induced by transient ischemia in rats. FASEB J. 2007; 21(14):3904–3916. [PubMed: 17628015]
43. Hu X, Le TH. Artifact reduction in EPI with phase-encoded reference scan. Magn. Reson. Med. 1996; 36(1):166–171. [PubMed: 8795036]
44. Jin T, Wang P, Zong X, Kim S-G. MR imaging of the amide-proton transfer effect and the pH-insensitive nuclear Overhauser effect at 9.4 T. Magn. Reson. Med. 2013; 69(3):760–770. [PubMed: 22577042]

45. Roeloffs, V.; Zaiss, M.; Bachert, P. An analytical approach towards pulsed-SL/CEST quantification; Proceedings of the 21st Annual Meeting ISMRM; Salt Lake City, UT, USA. 2013. p. 2546

46. Sun PZ, Farrar CT, Sorensen AG. Correction for artifacts induced by B(0) and B(1) field inhomogeneities in pH-sensitive chemical exchange saturation transfer (CEST) imaging. Magn. Reson. Med. 2007; 58(6):1207–1215. [PubMed: 17969015]

47. Haris M, Nath K, Cai K, Singh A, Crescenzi R, Kogan F, Verma G, Reddy S, Hariharan H, Melhem ER, Reddy R. Imaging of glutamate neurotransmitter alterations in Alzheimer's disease. NMR Biomed. 2012

48. Saar G, Zhang B, Ling W, Regatte RR, Navon G, Jerschow A. Assessment of glycosaminoglycan concentration changes in the intervertebral disc via chemical exchange saturation transfer. NMR Biomed. 2012; 25(2):255–261. [PubMed: 22253087]

49. Zu Z, Li K, Janve VA, Does MD, Gochberg DF. Optimizing pulsed-chemical exchange saturation transfer imaging sequences. Magn. Reson. Med. 2011; 66(4):1100–1108. [PubMed: 21432903]

50. Tee YK, Khrapitchev AA, Sibson NR, Payne SJ, Chappell MA. Evaluating the use of a continuous approximation for model-based quantification of pulsed chemical exchange saturation transfer (CEST). J. Magn. Reson. 2012; 222:88–95. [PubMed: 22858666]

51. Jones CK, Huang A, Xu J, Edden RAE, Schär M, Hua J, Oskolkov N, Zacà D, Zhou J, McMahon MT, Pillai JJ, van Zijl PCM. Nuclear Overhauser enhancement (NOE) imaging in the human brain at 7T. Neuroimage. 2013; 77:114–124. [PubMed: 23567889]

52. Henkelman RM, Huang X, Xiang QS, Stanisz GJ, Swanson SD, Bronskill MJ. Quantitative interpretation of magnetization transfer. Magn. Reson. Med. 1993; 29(6):759–766. [PubMed: 8350718]

53. Stanisz GJ, Odrobina EE, Pun J, Escaravage M, Graham SJ, Bronskill MJ, Henkelman RM. T1, T2 relaxation and magnetization transfer in tissue at 3 T. Magn. Reson. Med. 2005; 54(3):507–512. [PubMed: 16086319]

54. Singh A, Cai K, Haris M, Hariharan H, Reddy R. On B(1) inhomogeneity correction of in vivo human brain glutamate chemical exchange saturation transfer contrast at 7 T. Magn. Reson. Med. 2013; 69(3):818–824. [PubMed: 22511396]

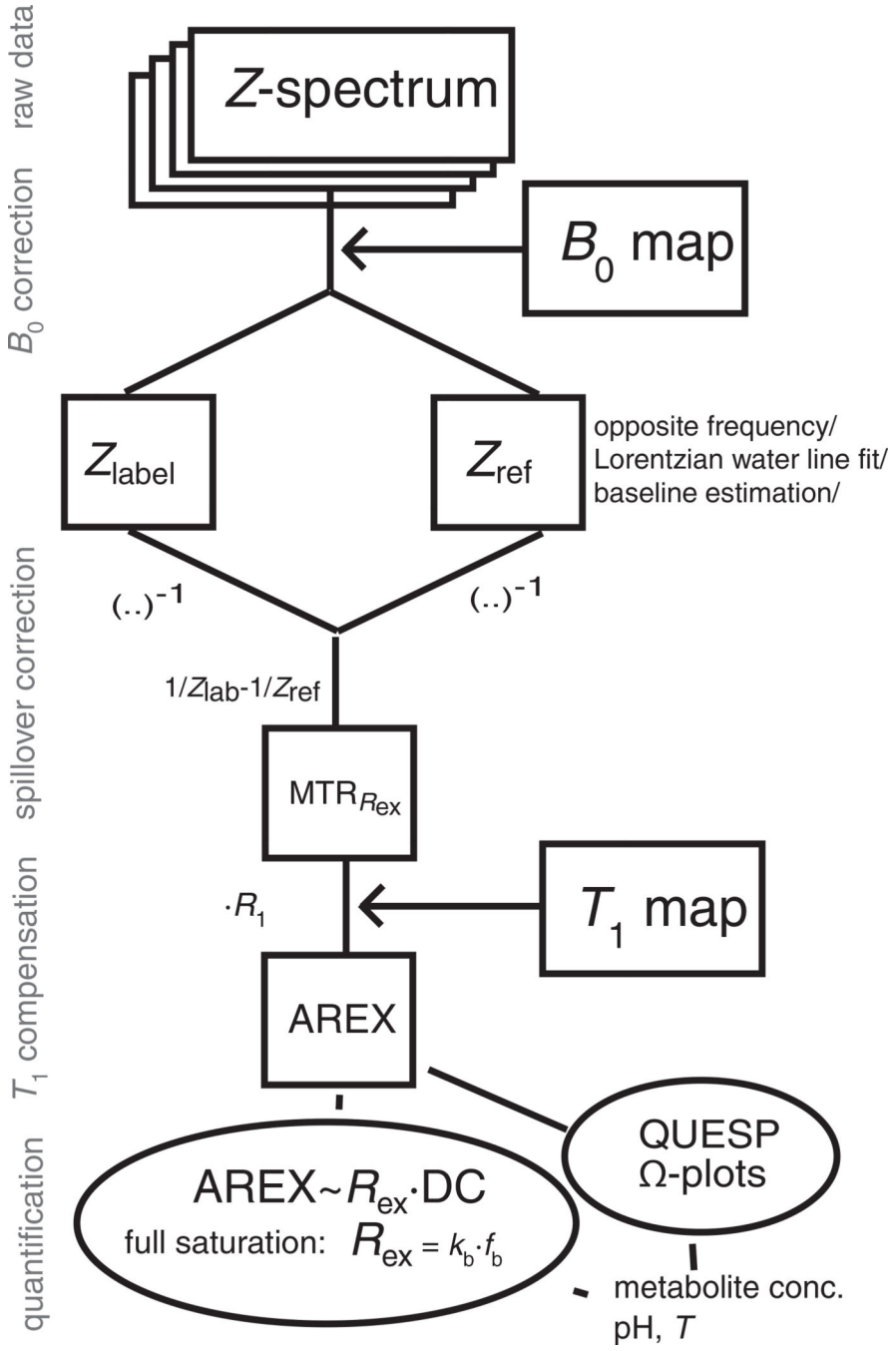

Figure 1.

Scheme of data evaluation for spillover- and T_1-compensated chemical exchange saturation transfer (CEST). Only simple matrix operations are performed to obtain the apparent exchange-dependent relaxation (AREX) contrast. The step of defining a suitable reference value Z_{ref} is crucial. DC, duty cycle; MTR_{Rex}, spillover-corrected magnetization transfer ratio yielding R_{ex}; QUESP, quantification of exchnage by saturation power.

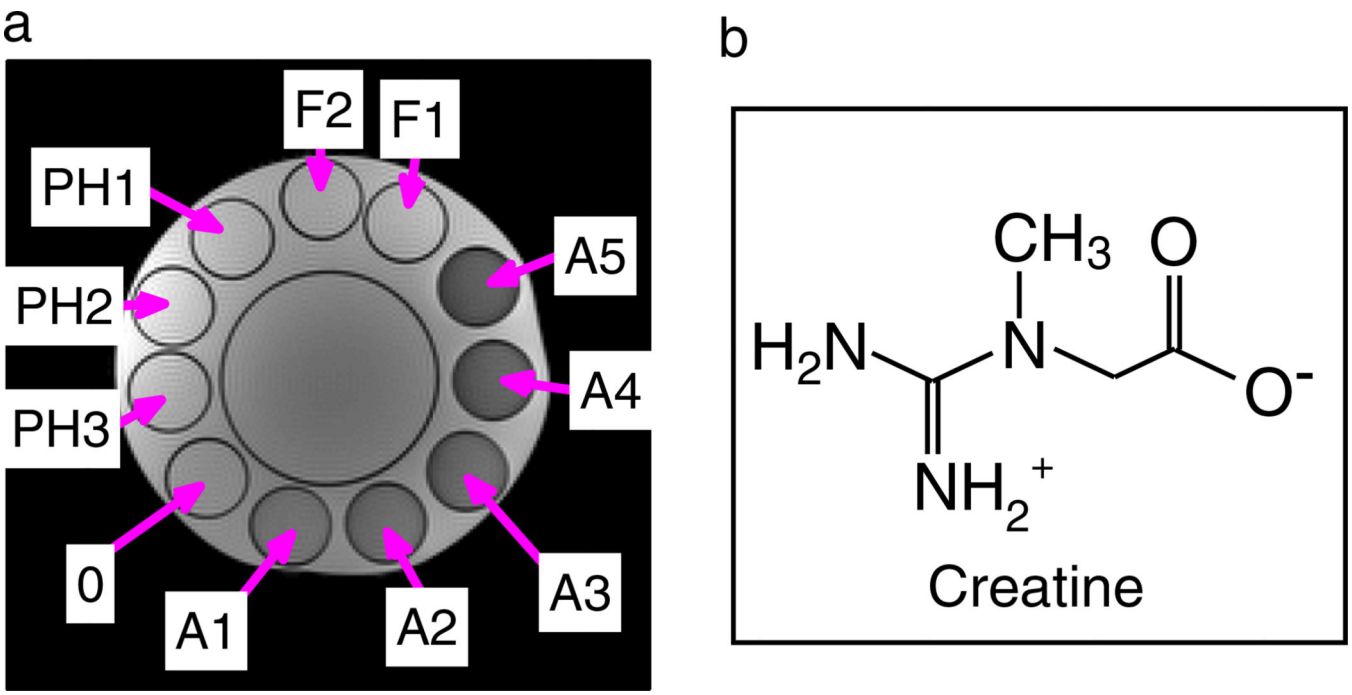

Figure 2.

(a) Turbo spin echo image of the phantom employed (for details, see Table 1). 0 is the reference solution with 55.5m$_M$ creatine and phosphate-buffered saline at pH 6.38 and without agar. The A*x* phantoms differ from phantom 0 by increasing agar concentration (0.2–1%). The PH*x* phantoms differ from phantom 0 by altered pH (6.2, 6.3, 6.6). The F*x* phantoms have different creatine concentrations [F1, 1/3 * 55.5 mM; F2, 2/3 * 55.5 mM]. (b) Zwitterionic form of aqueous creatine occurring at low pH.

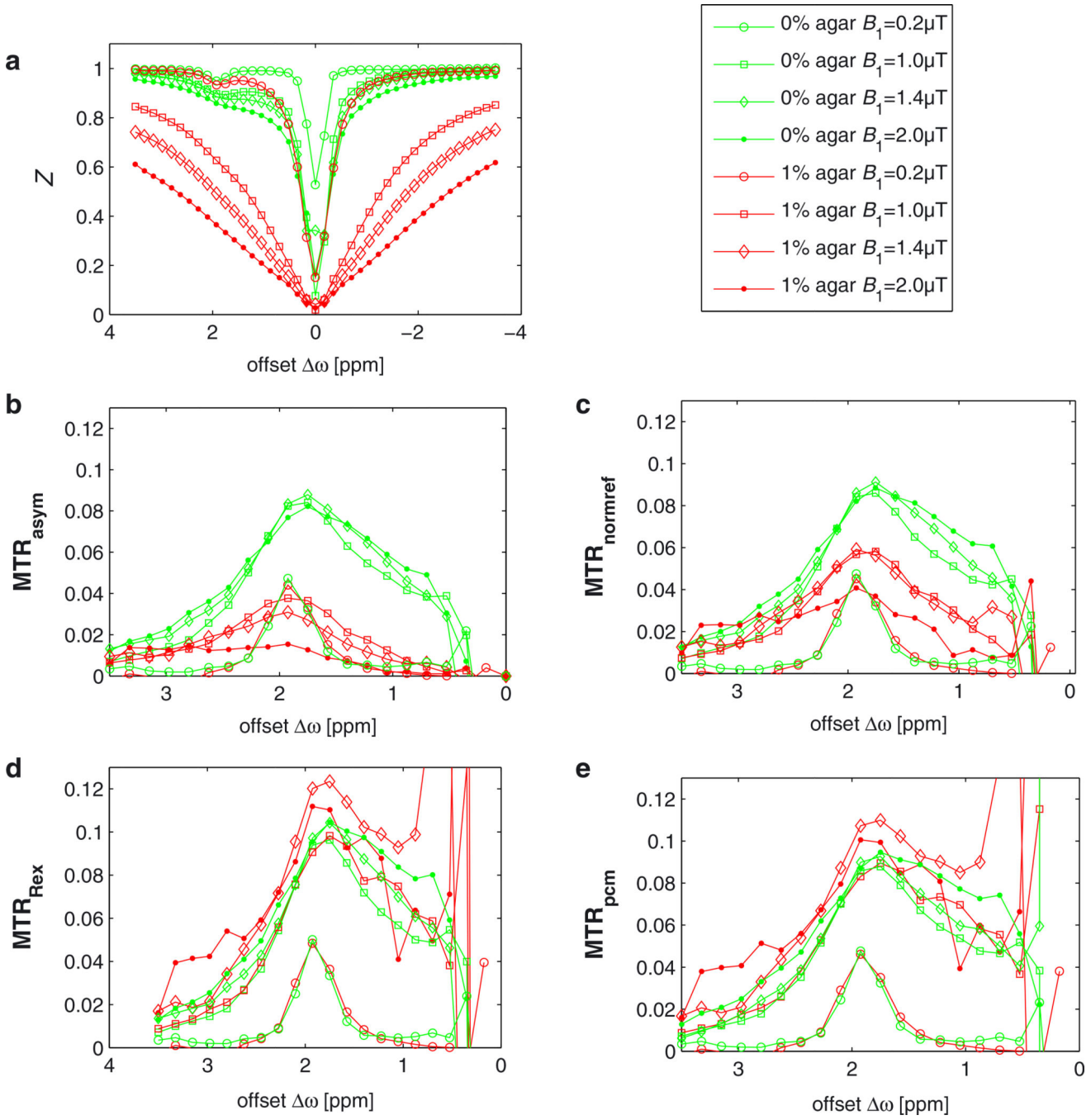

Figure 3.

(a) *Z*-spectra obtained with different B_1 values from creatine solutions with 1% agar (red lines, A5) and 0% agar (green lines, 0). Labeling increases with B_1, as does the direct saturation effect. For low B_1 of 0.2 μT (circles), the spillover effect is negligible (a), which explains why the curves overlap for all metrics (b–e). (b) MTR_{asym} shows strong spillover dilution in the solidified phantom (with agar), whereas MTR_{Rex} (d) and MTR_{pcm} (e) are able to correct the dilution so that aqueous and solidified phantoms yield almost the same effect. The spillover correction proposed by Liu *et al*. (35) (c) [Equation [8]] compensates spillover

partially. Error bars are omitted for better visibility; they increase strongly for higher spillover correction, as depicted in Fig. 10.

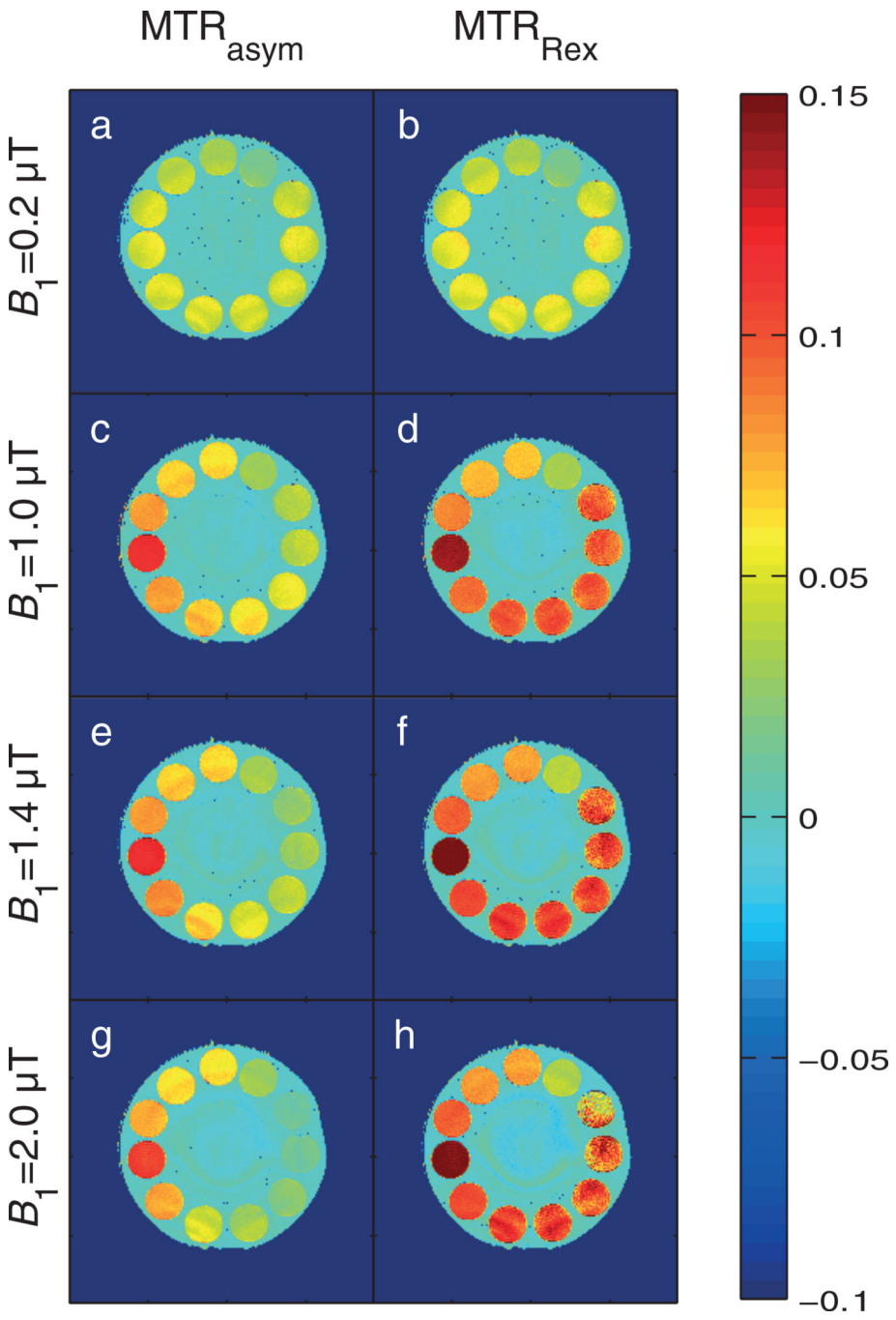

Figure 4.

Comparison of the normalizations MTR_{asym} (left column) and MTR_{Rex} (right column) for B_1 = 0.2, 1.0, 1.4 and 2.0 μT. In each case, the estimation of the chemical exchange saturation transfer (CEST) effect is higher for MTR_{Rex}. The phantoms with varying agar concentration (0, A1–A5) show similar contrast in MTR_{Rex}, whereas MTR_{asym} shows diluted contrast with increasing agar concentration. Differences in pH and creatine concentration are reflected in both magnetization transfer ratios (MTRs). Therefore, MTR_{Rex} has all the properties of a spillover correction.

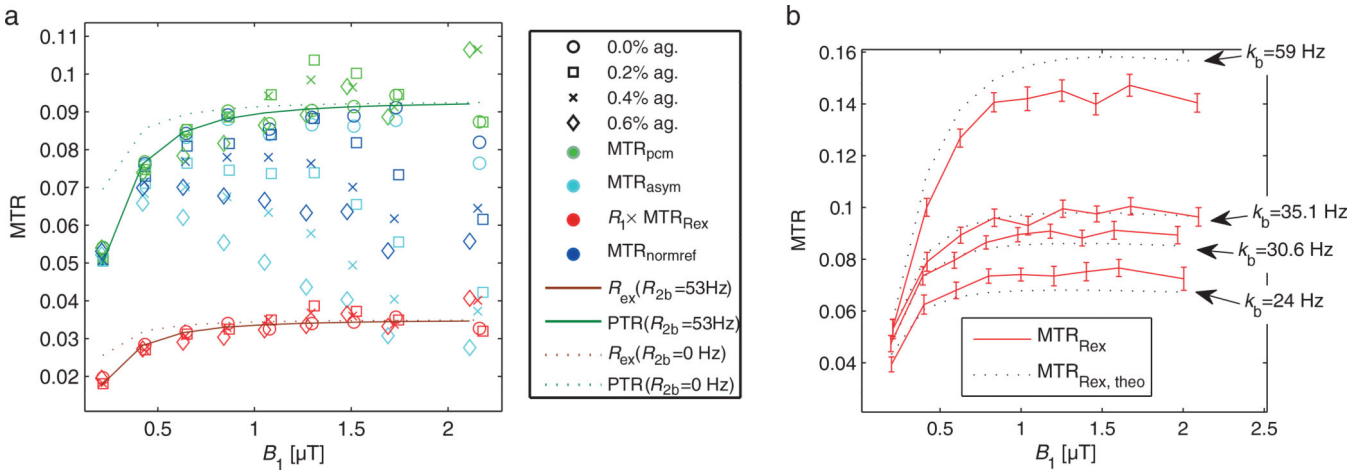

Figure 5.

(a) Region of interest (ROI) evaluation of ROIs in phantoms 0 and A1–A3 with the proposed spillover corrections. For all agar concentrations and B_1 values, both MTR_{pcm} (green) and MTR_{Rex} (red) appear to be in a narrow band around the control without agar (0). MTR_{asym} (cyan) and $MTR_{normref}$ (blue) show a much stronger decrease with increasing B_1 and agar. (b) MTR_{Rex} from data and from theory [Equation [15]] employing parameters of the numerical fit (Table 1, phantoms 0, PH1, PH2, and PH3). The curves match roughly and the dependence on k_b and B_1 is very similar.

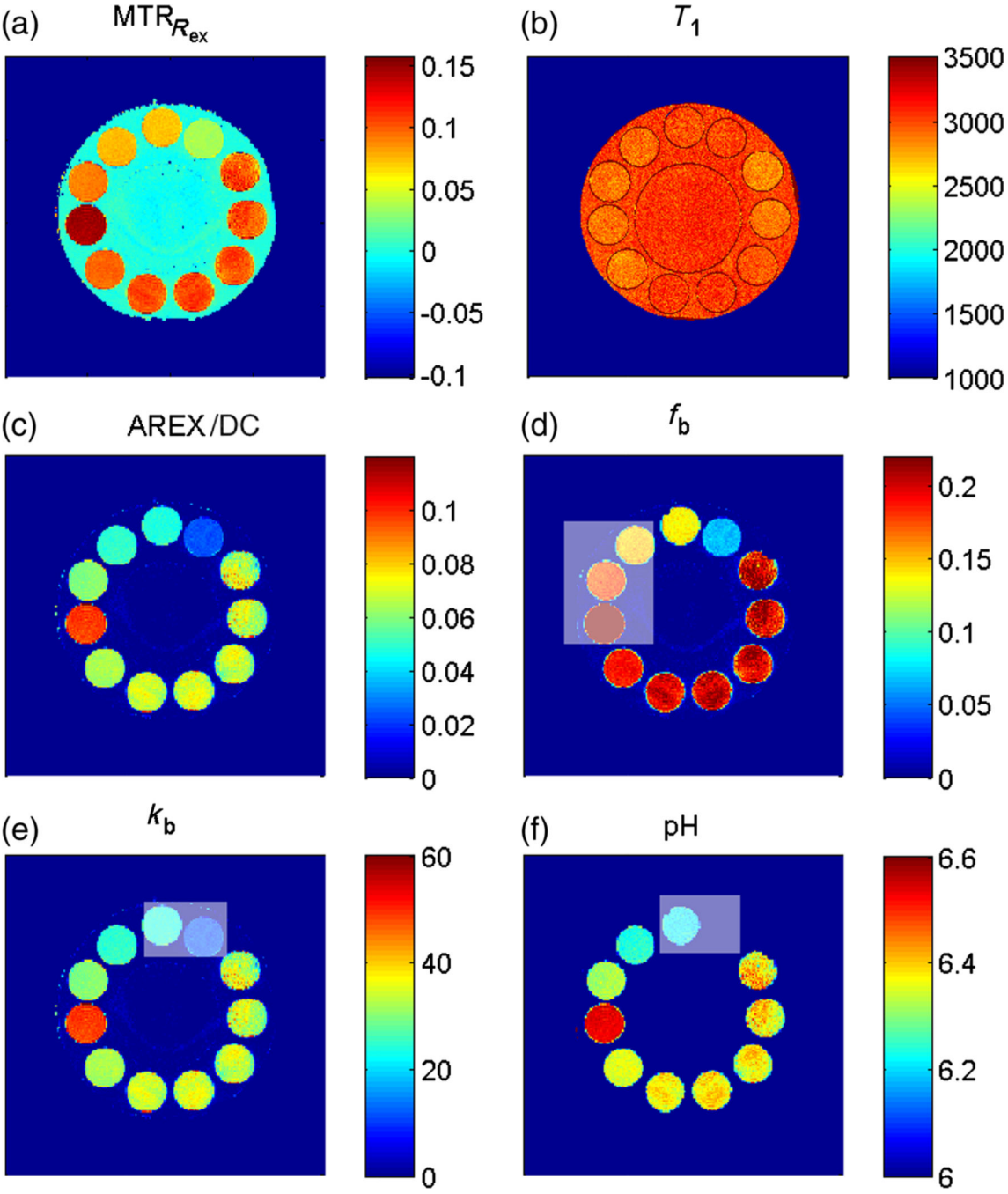

Figure 6.

Quantitative pulsed chemical exchange saturation transfer (CEST)-MRI. (a) MTR_{Rex} evaluated for B_1 = 1 μT. Employing the T_1 map (b), the spillover-corrected and T_1–compensated apparent exchange-dependent relaxation (AREX) map can be calculated (c). Under the assumption of full saturation, AREX/DC yields a k_a map. (d) f_b map employing the exchange rate for creatine k(pH 6.38, T = 19 °C) = 35 s^{-1}; it suggests that creatine has four exchanging protons. Using f_b = 0.2%, a k_b map (e) can be obtained from AREX, which correlates well with results from water exchange measurements. (f) Therefore, a pH(k_b) map

can be obtained using Equation [16]. Gray boxes indicate tubes in which either the concentration or pH was not constant.

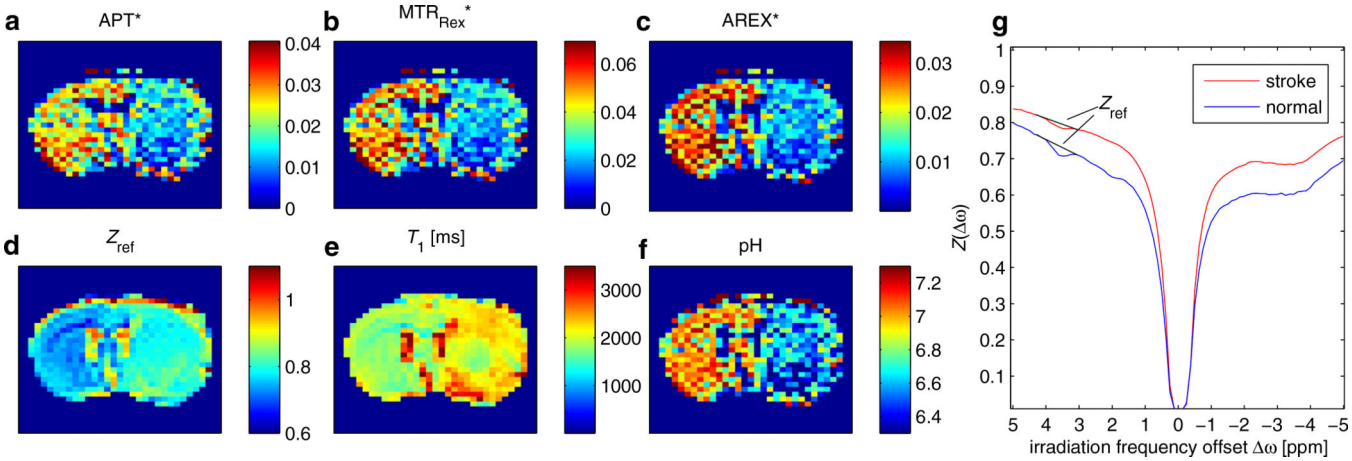

Figure 7.

Amide proton transfer (APT) contrast obtained by pulsed chemical exchange saturation transfer (CEST)-MRI of rat with acute stroke. APT contrast (a) is contaminated by T_1 (e) and spillover effects [visible in the reference image (d)]. After correction of spillover by the inverse metric MTR_{Rex}, the contrast between lesion and normal tissue increases (b). The T_1-corrected apparent exchange-dependent relaxation (AREX) evaluation yields a pure exchange-weighted contrast which shows even higher signal drop in the stroke lesion compared with normal tissue. (f) From AREX, an absolute pH map can easily be obtained by Equation [19]. For all CEST maps, the average of *Z*-values at 4.2 and 3 ppm was employed as a reference [Equation [21]], as illustrated by the baselines in the *Z*-spectra in (g). To achieve good visual comparison of the contrast, each magnetization transfer ratio (MTR) map was windowed from zero to two times the average value of all non-zero pixels. CEST echo planar imaging parameters were: matrix size, 64; TE = 28 ms. Pulse train parameters were: t_p = 12.5 ms; B_1 = 0.84 μT; duty cycle (DC) = 50%; flip angle, 180°; n = 200.

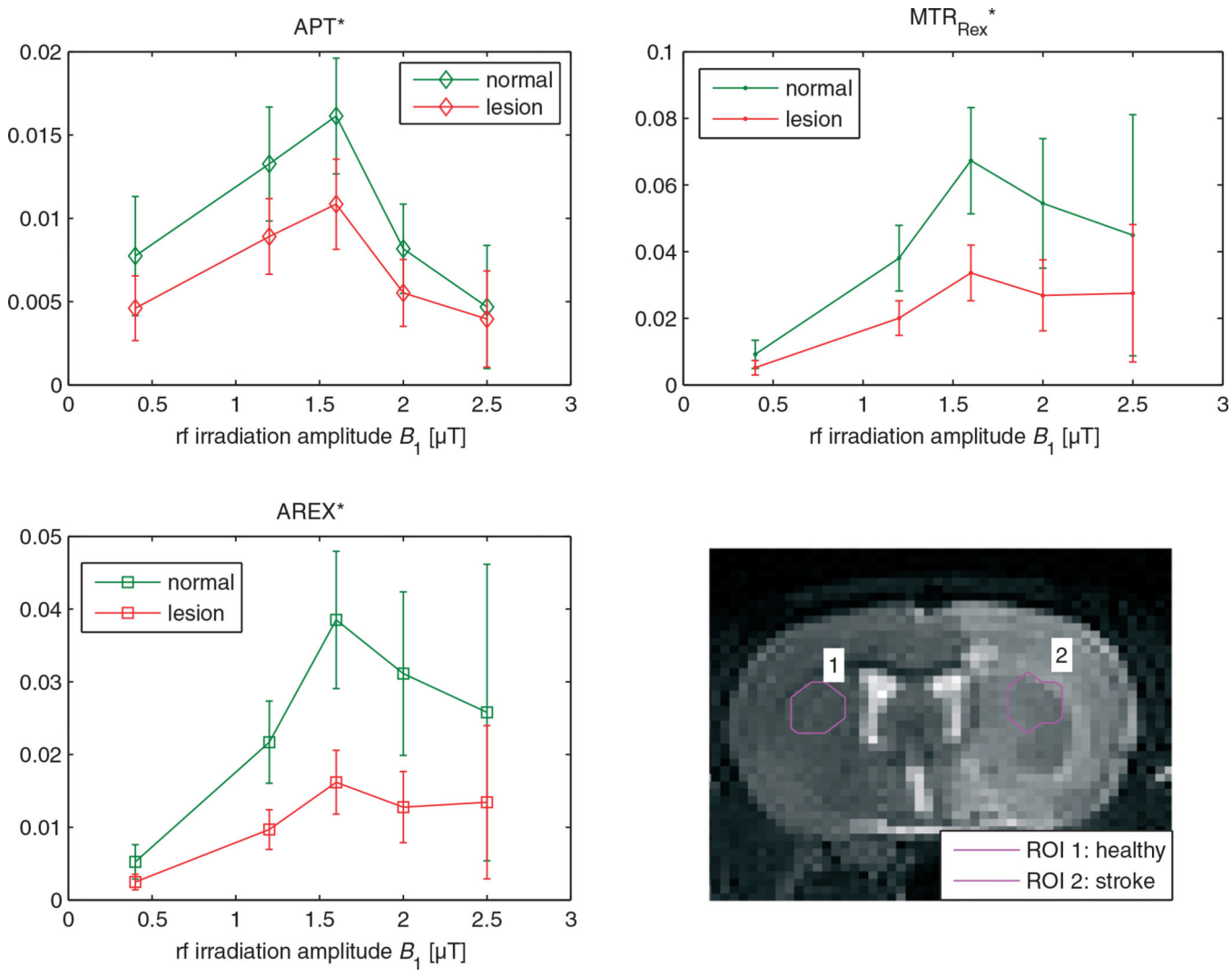

Figure 8.

Region of interest (ROI) evaluation of the three point methods: APT*, the spillover-corrected MTR$_{Rex}$ and the spillover- and T_1-compensated AREX. Similar to the phantom study, APT* shows a strong decrease with B_1 for values higher than 1.5 μT, whereas MTR$_{Rex}$ and AREX show a smaller decrease in signal for higher B_1. This pattern is similar to the phantom results (cf. Fig. 5) and indicates validity of the spillover correction. However, the plateau of the full-saturation limit is not reached, probably as a result of contamination of the reference scan. It is important to note that the differences between signals in the stroke lesion and normal tissue are much more significant after spillover correction and T_1 compensation. Under the assumption of equal amide concentrations in stroke and normal tissue, the signal drop reflects a change in exchange rate of about a factor of two. APT, amide proton transfer; AREX, apparent exchange-dependent relaxation; MTR$_{Rex}$, spillover-corrected magnetization transfer ratio yielding R_{ex}.

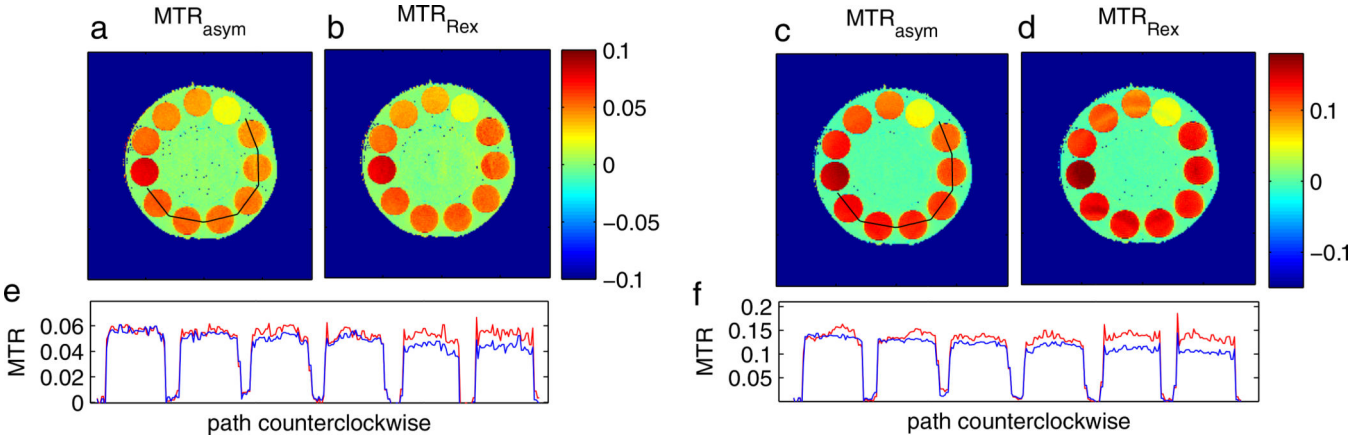

Figure 9.

MTR_{asym} (a, c) and the inverse approach MTR_{Rex} (b, d) for the practical relevant cases of non-steady-state saturation (t_{sat} = 3.1 s, B_1 = 0.5 μT, t_p = 100 ms, DC = 50%, n = 16) (a, b) and 180° pulsed saturation (180° pulses; B_1 = 0.48 μT, t_p = 25 ms, DC = 50%, n = 320) (c, d). Profiles along the path (counterclockwise) defined in (a) show that MTR_{Rex} (red line) corrects the decrease in MTR_{asym} (blue line) with increasing agar concentration.

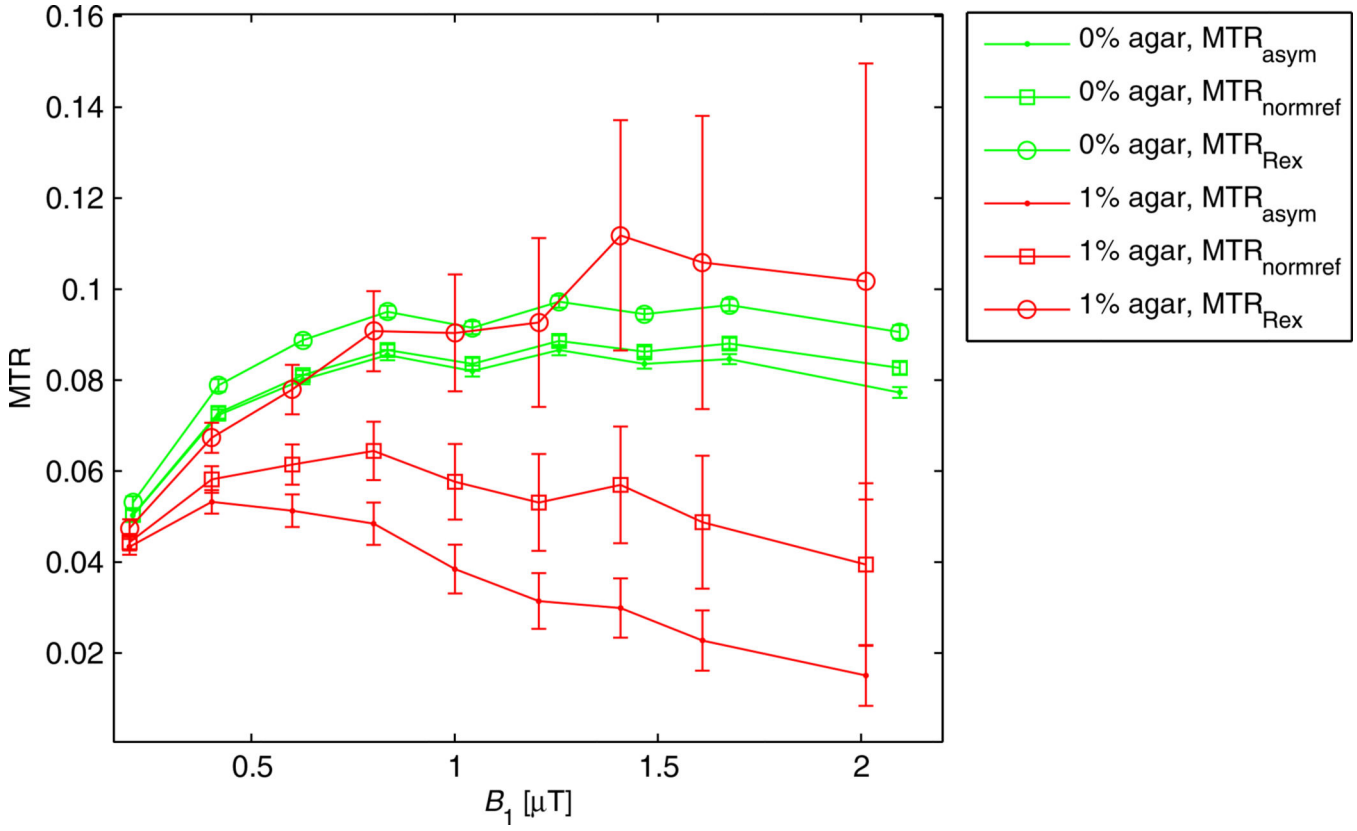

Figure 10.

Error estimation for the inverse metric. Absolute errors increase with increasing spillover effect. This results from the error propagation of the inverse metric. However, relative errors do not change and therefore the contrast-to-noise ratio is not affected. The systematic spillover deviation is traded with a statistical fluctuation. Original errors were scaled by a factor of one-third to improve visibility.

Table 1

Phantoms employed, as depicted in Fig. 2, with fitted values from region of interest (ROI) evaluations and exchange rates of creatine predicted by water exchange spectroscopy (WEX) studies (39). Fits by a two-pool Bloch–McConnell simulation were performed simultaneously for five *Z*-spectra obtained with B_1 = 0.2, 0.4, 0.6, 0.8 and 1.0 μT in each ROI

Phantom/ROI	pH	[Cr] (mM)	[Ag] (%)	k_b (WEX) (s^{-1})	k_b (CEST) (s^{-1})	f_b (%)	R_{2b} (s^{-1})	R_{2a} (s^{-1})	T_{1a} (s)
0	6.38	55.5	0	35.1	33.8	0.22	40.3	0.60	2.92
A1	6.38	55.5	0.2	35.1	–	–	–	2.47	2.99
A2	6.38	55.5	0.4	35.1	–	–	–	3.57	2.97
A3	6.38	55.5	0.6	35.1	–	–	–	4.82	2.92
A4	6.38	55.5	0.8	35.1	–	–	–	6.23	2.87
A5	6.38	55.5	1.0	35.1	–	–	–	7.58	2.83
F1	6.38	55.5 (1/3)	0	35.1	38.5	0.073	58	0.42	3.00
F2	6.38	55.5·(2/3)	0	35.1	46.5	0.13	53	0.42	2.99
PH1	6.21	55.5	0	23.72	31.6	0.18	49	0.44	2.91
PH2	6.32	55.5	0	30.6	34.8	0.20	48	0.43	2.93
PH3	6.61	55.5	0	59.6	63.0	0.21	54	0.46	2.93

−, missing fitting data when the two-pool model was insufficient.